Available online at www.sciencedirect.com
ScienceDirect
International Journal of Heat and Mass Transfer 51 (2008) 2980–2989
International Journal of HEAT and MASS TRANSFER
www.elsevier.com/locate/ijhmt

Buoyant convection in a parallelogrammic enclosure filled with a porous medium – General analysis and numerical simulations

Hun Sik Han, Jae Min Hyun *

Department of Mechanical Engineering, Korea Advanced Institute of Science and Technology, 373-1 Kusong-dong, Yusong-gu, Daejeon 305-701, South Korea

Received 24 May 2007; received in revised form 10 September 2007
Available online 7 November 2007

Abstract

A numerical study is made of buoyant convection in a parallelogrammic enclosure, which is filled with a porous medium. The enclosure is equipped with insulated non-vertical sidewalls and isothermal horizontal endwalls. The temperature at the top horizontal endwall is higher than the temperature at the bottom horizontal endwall. This provides a generally stable fluid stratification in the interior. Emphasis is given to the explicit role of local baroclinicity, which is induced in the immediate neighborhood of the non-vertical portions of the sidewalls. Comprehensive numerical solutions to the governing equations are acquired. The Boussinesq-fluid assumption is used, and the Brinkman-extended Darcy flow model is adopted in the momentum equation. In order to represent local thermal non-equilibrium, the two-equation model is utilized in the energy equation. A systematic scale analysis is performed, which produces descriptions of general flow and heat transport characteristics. These results are shown to be consistent with the detailed numerical solutions. Enhancement of heat transfer through the cavity is more pronounced as the inclination angle of the non-vertical sidewall increases.

Keywords: Buoyant convection; Porous medium; Baroclinicity; Heat transfer enhancement; Local thermal non-equilibrium

1. Introduction

Buoyant convection in a porous medium has been a subject of much interest. This is an important issue in many natural and industrial applications, such as geothermal energy modeling, solar power collector, pollutant in aquifers, cooling electronic systems, petroleum reservoirs and fuel cell, to name a few. The fundamental aspects of convective flows in a porous medium have been documented, e.g. [1–3].

The flow and heat transfer of a clear-fluid in buoyant convection in a rectangular enclosure, of which the vertical walls are maintained at two different temperatures and the horizontal walls are insulated, are benchmark problems (e.g. [4,5]). Expanding these studies, investigations on buoyant convection in a rectangular enclosure filled with a porous medium have been reported (e.g. [6–17]). Based on these studies, it is of interest to explore heat transfer features in more complex geometries. The prediction of heat transfer in irregular geometries is a topic of importance, and non-rectangular cavities are particularly relevant, e.g. [18–23].

Recently, Costa [24], Baytas and Pop [25] and Misirlioglu et al. [26,27] examined steady natural convection in a non-rectangular enclosure filled with a porous medium. These preceding efforts demonstrated that the geometrical shape is crucial in determining the fluid flow and heat transfer. Most of these studies are concerned with the case of differentially heated sidewalls, with insulated horizontal walls.

This paper intends to address the above two key issues, i.e., the case of a parallelogrammic porous-medium enclosure with thermally insulated sidewalls. The top and bottom horizontal walls are conductors. It is noted that the temperature at the top horizontal wall is higher than at the bottom horizontal wall. This leads to a generally stable stratification in the interior.

* Corresponding author. Tel.: +82 42 869 3012; fax: +82 42 869 3210.
E-mail address: jmhyun@kaist.ac.kr (J.M. Hyun).

0017-9310/$ - see front matter © 2007 Elsevier Ltd. All rights reserved.
doi:10.1016/j.ijheatmasstransfer.2007.09.015

Nomenclature

a_{sf}	interfacial surface area per unit volume
A	aspect ratio, H/L
Bi	Biot number, $h_{sf}a_{sf}H^2/k_e$
c_f	specific heat of fluid
Da	Darcy number, K/H^2
g	gravitational acceleration
h_{sf}	interstitial heat transfer coefficient
H	cavity height
k	thermal conductivity
K	permeability
L	cavity length
$\dot{m}$	mass flow rate
n^*	unit normal vector
Nu	local Nusselt number
$\overline{Nu}$	mean Nusselt number
p, P	dimensional and dimensionless pressure, $p\varepsilon^2H^2/\rho_f\kappa_e^2$
Pr	Prandtl number, ν_f/κ_e
Ra	Rayleigh number, $g\alpha\Delta TH^3/\kappa_e\nu_f$
Ra_m	modified Rayleigh number, $Kg\alpha\Delta TH/\kappa_e\nu_f$
T_0	average temperature, $(T_h + T_c)/2$
u, v	velocity components along x and y axes, respectively
U, V	dimensionless velocity components along X and Y axes, respectively, $(u,v)H/\kappa_e$
V	total system volume
x, y	Cartesian coordinates
X, Y	dimensionless Cartesian coordinates, $(x,y)/H$

Greek symbols

α	volumetric expansion coefficient
ΔT	temperature difference, $(T_h - T_c)/2$
ε	porosity
κ_e	effective thermal diffusivity, $k_e/\rho_f c_f$
λ	effective fluid-to-solid thermal conductivity ratio, $\varepsilon k_f/(1-\varepsilon)k_s$
ν_f	kinematic viscosity of fluid
θ	dimensionless temperature, $(T - T_0)/\Delta T$
ρ_f	density of fluid
φ	incline angle
ω, Ω	dimensional and dimensionless vorticity, $\omega H^2/\kappa_e$
ψ, Ψ	dimensional and dimensionless stream function, ψ/κ_e

Subscripts

c	cold
e	effective
f	fluid
h	hot
m	modified
s	solid

Buoyant convection in a porous-medium enclosure is customarily modeled under the assumption of local thermal equilibrium between the fluid phase and the solid phase, which leads to the one-equation model in the energy equation (e.g. [6–15,24–27]). Obviously, the one-equation model is simple and straightforward. However, the one-equation model becomes less accurate as the temperature difference between the solid and fluid phases increases. In this case, the two-equation model will be used, which treats the solid phase and the fluid phase separately. Kim and Jang [16] and Khashan et al. [17] gave discussions on the utility and limitations of the local thermal equilibrium assumption in forced convection and in the Benard convection.

The intention of this paper is heat transfer enhancement, which is driven by non-vertical insulated sidewalls. To present a general description of the flow field, a scale analysis is performed. A comprehensive numerical study will be undertaken to obtain the flow details.

2. Formulation and numerical model

Consider a parallelogrammic porous-medium enclosure (width L and height H), filled with a viscous, Boussinesq-fluid. The non-vertical sidewalls are thermally insulated, and the temperatures at the top and bottom horizontal walls are, respectively, T_h and T_c, with $\Delta T \equiv (T_h - T_c)/2 > 0$, as shown in Fig. 1b. The present configuration is top-heated, and it should be distinguished from the bottom-heated Benard-type setup.

The vorticity equation describes the evolution of the vorticity of a fluid element as it moves around and can be derived from the curl of momentum equation. In general vector form, it may be expressed as follows:

$$\frac{\partial\vec{\omega}}{\partial t} + (\vec{u}\cdot\nabla)\vec{\omega} = (\vec{\omega}\cdot\nabla)\vec{u} - \frac{\nabla p\times\nabla\rho}{\rho^2} + \nu\nabla^2\vec{\omega} + \nabla\times\vec{b}, \tag{1}$$

where $\vec{\omega}$, $\vec{u}$, ρ, p and $\vec{b}$ denote the vorticity vector, velocity vector, density, pressure and body force term, respectively. If the geometrical shape of a cavity is rectangular, as sketched in Fig. 1a, there are no fluid motions, and heat transfer is purely conductive. In this case, the baroclinic term in the vorticity equation (Eq. (1)), i.e., $(\nabla p\times\nabla\rho)/\rho^2$, is identically zero, and the whole cavity is vorticity-free. Subsequently, the appropriately defined Nusselt number $\overline{Nu}$ at the horizontal wall is unity. However, in the case of a parallelogrammic cavity, the existence of non-vertical

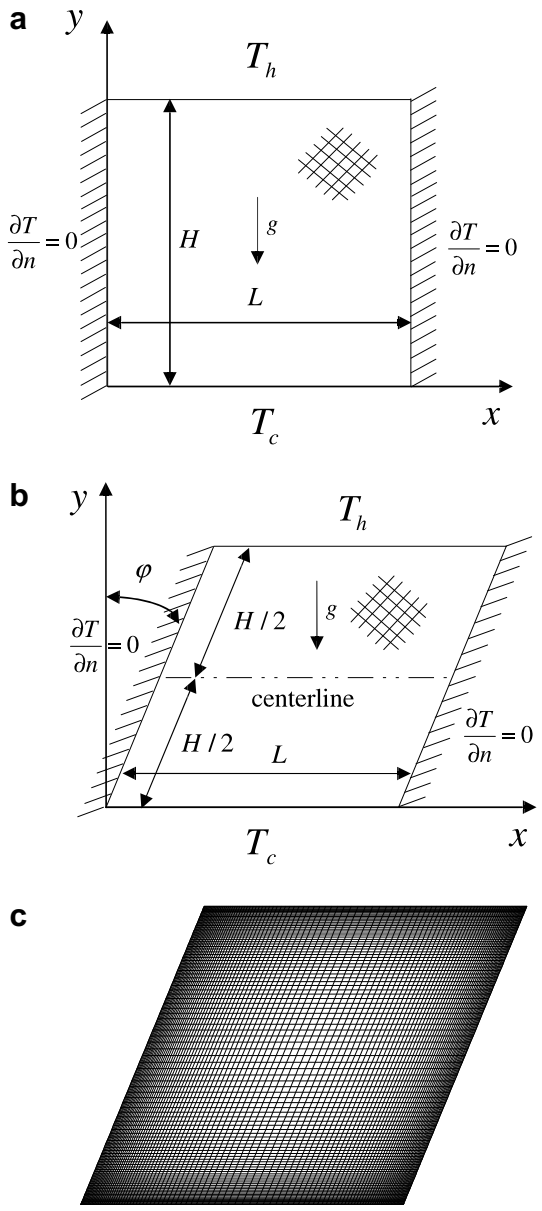

Fig. 1. Schematic diagram of the flow configuration. (a) Rectangular porous-medium enclosure; (b) parallelogrammic porous-medium enclosure; (c) 80×80 staggered and stretched grid size.

portions of the sidewall brings forth fluid flows because of the non-vanishing baroclinic term, i.e., $(\nabla p \times \nabla \rho)/\rho^2 \neq 0$. As a result, the overall heat transfer from the top to bottom horizontal walls is augmented, in comparison to the strictly conductive case. The mechanism of this baroclinically induced buoyant convective heat transfer was examined in detail by Kim and Hyun [21].

For the present mathematical formulation, the following assumptions are invoked: the porous medium is isotropic and homogeneous; the properties of the fluid and porous medium are constant; the Boussinesq-fluid approximation is used; the Brinkman-extended Darcy flow model is adopted in the momentum equation since the inertial effect, i.e., the Forchheimer term, is negligible; the two-equation model is employed in the energy equation under the assumption of local thermal non-equilibrium. When using the Brinkman-extended Darcy flow model, it is assumed that the effective viscosity is the same as the fluid viscosity. Strictly speaking, this may not be the case. However, due to the lack of experimental data, it has become customary to make this assumption [7–9,11,13,15–17].

The governing equations based on volume-averaging method, are [17]:

$$\frac{\partial u}{\partial x}+\frac{\partial \mathrm{v}}{\partial y}=0, \tag{2}$$

$$\frac{\rho_\mathrm{f}}{\varepsilon}\left\{u\frac{\partial}{\partial x}\left(\frac{u}{\varepsilon}\right)+v\frac{\partial}{\partial y}\left(\frac{u}{\varepsilon}\right)\right\} = -\frac{1}{\varepsilon}\frac{\partial}{\partial x}(p\varepsilon)+\frac{\mu_\mathrm{f}}{\varepsilon}\left(\frac{\partial^2 u}{\partial x^2}+\frac{\partial^2 u}{\partial y^2}\right)-\frac{\mu_\mathrm{f}}{K}u, \tag{3}$$

$$\frac{\rho_\mathrm{f}}{\varepsilon}\left\{u\frac{\partial}{\partial x}\left(\frac{v}{\varepsilon}\right)+v\frac{\partial}{\partial y}\left(\frac{v}{\varepsilon}\right)\right\} = -\frac{1}{\varepsilon}\frac{\partial}{\partial y}(p\varepsilon)+\frac{\mu_\mathrm{f}}{\varepsilon}\left(\frac{\partial^2 v}{\partial x^2}+\frac{\partial^2 v}{\partial y^2}\right)+\rho_\mathrm{f} g\alpha(T_\mathrm{f}-T_0)-\frac{\mu_\mathrm{f}}{K}v, \tag{4}$$

$$(\rho c)_\mathrm{f}\left(u\frac{\partial T_\mathrm{f}}{\partial x}+v\frac{\partial T_\mathrm{f}}{\partial y}\right) = \varepsilon k_\mathrm{f}\left(\frac{\partial^2 T_\mathrm{f}}{\partial x^2}+\frac{\partial^2 T_\mathrm{f}}{\partial y^2}\right)+h_\mathrm{sf}a_\mathrm{sf}(T_\mathrm{s}-T_\mathrm{f}), \tag{5}$$

$$0=(1-\varepsilon)k_\mathrm{s}\left(\frac{\partial^2 T_\mathrm{s}}{\partial x^2}+\frac{\partial^2 T_\mathrm{s}}{\partial y^2}\right)+h_\mathrm{sf}a_\mathrm{sf}(T_\mathrm{f}-T_\mathrm{s}), \tag{6}$$

where x and y are the Cartesian coordinates pointing in the horizontal and vertical directions, respectively; u and v represent the volume averaged velocity components in the x and y directions, respectively; p is the pressure; T_f and T_s stand for the temperatures of fluid and of solid, respectively; ρ_f, μ_f, k_f, k_s, a_sf, h_sf, ε, α, g and K denote the density of fluid, dynamic viscosity of fluid, thermal conductivity of fluid, thermal conductivity of solid, interfacial surface area per unit volume, interstitial heat transfer coefficient, porosity, volumetric expansion coefficient, gravitational acceleration and permeability, respectively.

The associated boundary conditions are expressed as

$$\begin{aligned}
&u=v=0 \text{ at all solid walls,}\\
&T_\mathrm{f}=T_\mathrm{s}=T_\mathrm{h}\ [=T_0+\Delta T]\\
&\quad\text{at the top horizontal endwall,}\\
&T_\mathrm{f}=T_\mathrm{s}=T_\mathrm{c}\ [=T_0-\Delta T]\\
&\quad\text{at the bottom horizontal endwall,}\\
&\frac{\partial T_\mathrm{f}}{\partial n^*}=\frac{\partial T_\mathrm{s}}{\partial n^*}=0 \text{ at the sidewalls,}
\end{aligned} \tag{7}$$

where n^* denotes the unit normal vector.

In the course of computations, Eqs. (2)–(7) were non-dimensionalized in the following fashion [9,17,20,21]:

$$(X,Y)=\frac{(x,y)}{H},\quad (U,V)=(u,v)\frac{H}{\kappa_e},\quad P=\frac{p\varepsilon^2H^2}{\rho_f\kappa_e^2},$$
$$\theta_f=\frac{T_f-T_0}{\Delta T},\quad \theta_s=\frac{T_s-T_0}{\Delta T},\quad \Psi=\frac{\psi}{\kappa_e},$$
$$\Omega=\frac{\omega H^2}{\kappa_e},\quad Da=\frac{K}{H^2},\quad Ra=\frac{g\alpha\Delta TH^3}{\kappa_e\nu_f},$$
$$Ra_m=\frac{Kg\alpha\Delta TH}{\kappa_e\nu_f},\quad Pr=\frac{\nu_f}{\kappa_e},$$
$$\lambda=\frac{\varepsilon k_f}{(1-\varepsilon)k_s},\quad Bi=\frac{h_{sf}a_{sf}H^2}{k_e},\tag{8}$$

where Ψ and Ω represent the dimensionless stream function and dimensionless vorticity, respectively; Da, Ra, Ra_m, Pr, λ and Bi are the Darcy number, Rayleigh number, modified Rayleigh number, Prandtl number, effective fluid-to-solid thermal conductivity ratio and Biot number, respectively. The effective thermal diffusivity κ_e is set equal to $k_e/(\rho_f c_f)$, where $k_e=\varepsilon k_f+(1-\varepsilon)k_s$. The Biot number, Bi, is a measure of the conductive thermal resistance by the porous medium in comparison to the interstitial convective thermal resistance between the fluid and solid phases. In passing, it is mentioned that the functional dependence of Bi on Ra is not clear a priori. Therefore, treating Bi as independent parameter could result in a simplification of the problem. Also, the modified Rayleigh number Ra_m is defined as $Ra\cdot Da$.

The governing equations, in properly non-dimensionalized form, are:

$$\frac{\partial U}{\partial X}+\frac{\partial V}{\partial Y}=0,\tag{9}$$
$$U\frac{\partial U}{\partial X}+V\frac{\partial U}{\partial Y}=-\frac{\partial P}{\partial X}+\varepsilon Pr\left(\frac{\partial^2U}{\partial X^2}+\frac{\partial^2U}{\partial Y^2}\right)-\varepsilon^2\frac{Pr}{Da}U,\tag{10}$$
$$U\frac{\partial V}{\partial X}+V\frac{\partial V}{\partial Y}=-\frac{\partial P}{\partial Y}+\varepsilon Pr\left(\frac{\partial^2V}{\partial X^2}+\frac{\partial^2V}{\partial Y^2}\right)-\varepsilon^2\frac{Pr}{Da}V+\varepsilon^2RaPr\theta_f,\tag{11}$$
$$U\frac{\partial\theta_f}{\partial X}+V\frac{\partial\theta_f}{\partial Y}=\frac{1}{1+\lambda^{-1}}\left(\frac{\partial^2\theta_f}{\partial X^2}+\frac{\partial^2\theta_f}{\partial Y^2}\right)+Bi(\theta_s-\theta_f),\tag{12}$$
$$0=\frac{1}{1+\lambda}\left(\frac{\partial^2\theta_s}{\partial X^2}+\frac{\partial^2\theta_s}{\partial Y^2}\right)+Bi(\theta_f-\theta_s).\tag{13}$$

Expressed in the vorticity-stream function formulation, the governing equations, written in non-dimensionalized form, are:

$$\frac{\partial^2\Psi}{\partial X^2}+\frac{\partial^2\Psi}{\partial Y^2}=-\Omega,\tag{14}$$
$$U\frac{\partial\Omega}{\partial X}+V\frac{\partial\Omega}{\partial Y}=\varepsilon Pr\left(\frac{\partial^2\Omega}{\partial X^2}+\frac{\partial^2\Omega}{\partial Y^2}\right)-\varepsilon^2\frac{Pr}{Da}\Omega+\varepsilon^2RaPr\frac{\partial\theta_f}{\partial X},\tag{15}$$
$$U\frac{\partial\theta_f}{\partial X}+V\frac{\partial\theta_f}{\partial Y}=\frac{1}{1+\lambda^{-1}}\left(\frac{\partial^2\theta_f}{\partial X^2}+\frac{\partial^2\theta_f}{\partial Y^2}\right)+Bi(\theta_s-\theta_f),\tag{16}$$
$$0=\frac{1}{1+\lambda}\left(\frac{\partial^2\theta_s}{\partial X^2}+\frac{\partial^2\theta_s}{\partial Y^2}\right)+Bi(\theta_f-\theta_s),\tag{17}$$

where U and V denote the dimensionless velocity components in the x and y directions, respectively; Ω represents the dimensionless vorticity; i.e.,

$$U=\frac{\partial\Psi}{\partial Y},\quad V=-\frac{\partial\Psi}{\partial X},\quad \Omega=\frac{\partial V}{\partial X}-\frac{\partial U}{\partial Y}.\tag{18}$$

The associated boundary conditions, in properly non-dimensionalized form, are:

$$\begin{aligned}&U=V=0 \text{ at all solid walls,}\\ &\theta_f=\theta_s=\theta_h=1.0\\ &\quad\text{at the top horizontal endwall,}\\ &\theta_f=\theta_s=\theta_c=-1.0\\ &\quad\text{at the bottom horizontal endwall,}\\ &\frac{\partial\theta_f}{\partial n}=\frac{\partial\theta_s}{\partial n}=0 \text{ at the sidewalls.}\end{aligned}\tag{19}$$

Numerical solutions were acquired to the governing equations (Eqs. (9)–(13)). The well-established finite volume method (FVM) based on the SIMPLER algorithm, together with the QUICK scheme, was adopted [28,29]. A body-fitted coordinate transform was implemented in order to deal with the complexity of geometrical shape. To obtain the steady state solutions, the governing equations were iteratively solved until the rate of relative change in velocities and temperatures decreased below 10^{-6} at all nodes. Grid-convergence tests were performed for a variety of grid sizes as illustrated in Table 1. A grid size of 80×80, as shown in Fig. 1c, was selected on the basis of execution time and accuracy trade-off. A staggered and stretched grid was deployed to cluster mesh points near the walls. A series of computations were repeated for benchmark problems to verify the reliability and resolution of the code. The present results were validated by using the results of a parallelogrammic enclosure of a clear-fluid [21] and the Darcy flow model solutions [25,26], as shown in Table 2. The code was executed under the condition of $\varepsilon=1.0$, $Da=\infty$, $\lambda=\infty$ and $Bi=0$ for comparison with the clear-fluid model in the case of $A=1.0$, $Pr=7.0$ and $\varphi=30°$. For comparison with the Darcy flow model, the parameter was fixed at $Da=10^{-6}$ to minimize the boundary effect, i.e., Brinkman

Table 1
Grid size dependency analysis on the mean Nusselt number and the maximum stream function values for the case $A=1.0$, $\varphi=30°$, $\varepsilon=0.9$, $Pr=1.0$, $Ra=10^8$ and $Da=10^{-3}$

Grid size	$\overline{Nu}$		ψ_{max}	
20×20	1.1577	(–)	0.6632	(–)
40×40	1.1488	(0.78%)	0.6605	(0.411%)
60×60	1.1467	(0.18%)	0.6600	(0.079%)
80×80	1.1458	(0.08%)	0.6598	(0.031%)
100×100	1.1453	(0.04%)	0.6597	(0.016%)
120×120	1.1450	(0.03%)	0.6596	(0.009%)

Figures in the parentheses are the absolute relative error between grid size.

Table 2
Comparison of the mean Nusselt number

Authors	$Ra = 10^6$	$Ra = 10^7$	$Ra = 10^8$
(a) Clear-fluid model in a parallelogrammic enclosure			
Kim and Hyun [21]	1.1241	1.1384	1.1467
Present study	1.1235	1.1379	1.1458
	$Ra_m = 10^1$	$Ra_m = 10^2$	$Ra_m = 10^3$
(b) Darcy flow model in a square enclosure			
Baytas and Pop [25]	1.079	3.16	14.06
Misirlioglu et al. [26]	1.119	3.05	13.15
Present study ($Da = 10^{-6}$)	1.076	3.07	13.27

term. It is seen from Table 2 that the present and the previous results are in good agreement. Therefore, it can be concluded that the numerical methodologies used are robust and accurate.

In the present study, the parameter ranges were $30° \leqslant \varphi \leqslant 60°$, $10^6 \leqslant Ra \leqslant 10^8$, $10^{-5} \leqslant Da \leqslant 10^{-2}$, $0.1 \leqslant \lambda \leqslant 1.0$ and $1 \leqslant Bi \leqslant 100$, and $A = 1.0$, $Pr = 1.0$ and $\varepsilon = 0.9$. To process the numerical data, it is useful to introduce

$$\mathrm{LTD} \equiv |\theta_s - \theta_f|, \quad \mathrm{LTD}_{max} \equiv \mathrm{MAX}(\mathrm{LTD}),$$
$$\text{Percentage } \mathrm{LTD}_{max} \equiv \frac{\mathrm{LTD}_{max}}{\theta_h - \theta_c} \times 100. \tag{20}$$

In the above, LTD denotes the absolute value of the local temperature difference between the fluid and solid phases in the entire cavity; LTD_{max} represents the maximum value of local temperature difference. The local Nusselt number Nu at the bottom horizontal endwall is given as

$$Nu \equiv \frac{L}{2H}\left[\frac{1}{1+\lambda^{-1}}\frac{\partial\theta_f}{\partial Y} + \frac{1}{1+\lambda}\frac{\partial\theta_s}{\partial Y}\right]_{Y=0}, \tag{21}$$

and the mean Nusselt number is defined as

$$\overline{Nu} \equiv \int_0^1 Nu\,dX. \tag{22}$$

3. Results and discussion

3.1. Characteristics of heat transfer using the thermal non-equilibrium model

Fig. 2 exhibits exemplary plots of stream function, fluid temperature, solid temperature and local temperature difference in the case of $\varphi = 30°$, $Bi = 10$, $\lambda = 0.1$, $Ra = 10^7$ and $Da = 10^{-4}$. As shown in Fig. 2a, the main flow is characterized by a counter-clockwise circulation cell, and the fluid flow of boundary layer-type is generated by local baroclinicity. Temperature distributions of fluid and of solid are shown in Fig. 2b and c. The fluid phase is strongly stratified because of the convective effect, while stratification is weak in the solid phase due to the absence of advection term in the energy equation for the solid phase, see Eq. (6). Therefore, it is discernible that the solid phase is dominated by conduction. The temperature difference between the fluid and solid phases, i.e., LTD, is sketched in Fig. 2d. The LTD_{max} is located in the boundary layer where the fluid flow is generated, while LTD is meager in the interior core where the fluid motion is weak.

3.2. Scale analysis

As the system approaches the steady state, in the thermal boundary layer, the convection term $(\rho c)_f v \Delta T_f / H$ in

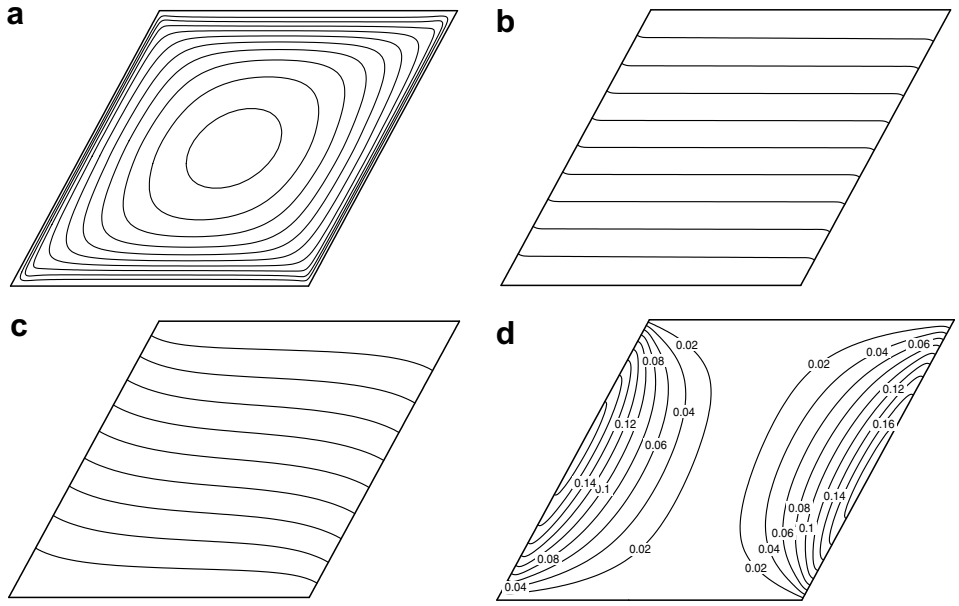

Fig. 2. Fluid flow and heat transfer features. $\varphi = 30°$, $Bi = 10$, $\lambda = 0.1$, $Ra = 10^7$, $Da = 10^{-4}$. (a) Flow field. The number of contours is 10, $\Delta\Psi = 0.02$; (b) fluid temperature field. The number of contours is 9, $\Delta\theta_f = 0.2$; (c) solid temperature field. The number of contours is 9, $\Delta\theta_s = 0.2$ and (d) local temperature difference field. The number of contours is 9, $\Delta\mathrm{LTD} = 0.02$.

the energy equation for the fluid phase (Eq. (5)) is balanced by the conduction term $(1-\varepsilon)k_s\Delta T_s/\delta_{T_s}^2$ in the energy equation for the solid phase (Eq. (6)) under the assumption of $(\delta_{T_f}/\delta_{T_s})^2(\Delta T_s/\Delta T_f) \sim O(1)$. This gives

$$v \sim \frac{\kappa_e}{1+\lambda}\frac{H}{\delta_{T_f}^2}. \tag{23}$$

In the momentum equation (Eq. (4)), the advection term $\rho_f v^2/\varepsilon^2 H$, the viscous term $\mu_f v/\varepsilon\delta_{T_f}^2$ and the Darcy term $\mu_f v/K$ are the candidates to balance the buoyancy term at the steady state. The ratio of the advection term to the viscous term, with the scale of Eq. (23), is $O((\varepsilon(1+\lambda)Pr)^{-1})$. Therefore, the advection term is neglected for high Prandtl number $Pr \geqslant 1$, $\varepsilon \sim O(1)$ and $\lambda > 0$. In the boundary layer, the buoyancy term is balanced by the viscous term or the Darcy term.

If the Darcy term is insignificant in the thermal boundary layer, the buoyancy term is balanced with the viscous term, namely

$$\rho_f g\alpha\Delta T_f \sim \frac{\mu_f}{\varepsilon}\frac{v}{\delta_{T_f}^2}. \tag{24}$$

With Eqs. (23) and (24), the velocity and length scales are

$$v \sim \frac{\kappa_e}{H}\left(\frac{\varepsilon}{1+\lambda}Ra\right)^{1/2}, \quad \delta_{T_f} \sim \frac{H}{(\varepsilon(1+\lambda)Ra)^{1/4}}. \tag{25}$$

In order to neglect the Darcy term, the Darcy term must be smaller than the viscous term, namely

$$\mu_f v/K \ll \mu_f v/\varepsilon\delta_{T_f}^2. \tag{26}$$

With Eqs. (23) and (25), Eq. (26) yields the criterion,

$$1 \ll \varepsilon^{-1/2}(1+\lambda)^{1/2}Ra^{1/2}Da. \tag{27}$$

In the opposite case, if the viscous term is unimportant in the thermal boundary layer, the buoyancy term is balanced with the Darcy term, namely

$$\rho_f g\alpha\Delta T_f \sim \frac{\mu_f}{K}v. \tag{28}$$

With Eqs. (23) and (28), the velocity and length scales are

$$v \sim RaDa\frac{\kappa_e}{H}, \quad \delta_{T_f} \sim \frac{H}{((1+\lambda)RaDa)^{1/2}}. \tag{29}$$

To neglect the viscous term, the viscous term $\mu_f v/\varepsilon\delta_{T_f}^2$ must be smaller than the Darcy term $\mu_f v/K$, which yields the criterion, with Eqs. (23) and (29):

$$\varepsilon^{-1/2}(1+\lambda)^{1/2}Ra^{1/2}Da \ll 1. \tag{30}$$

To identify the prominent dynamical effects, the sizes of the individual terms divided by $Ra \cdot Pr$ in the non-dimensionalized vertical momentum equation (Eq. (11)), evaluated along the centerline in the left-half of the cavity, are displayed in Fig. 3 for the exemplary case of $\varphi = 30°$, $Bi = 100$ and $\lambda = 0.1$. The setup of $Da = 10^{-3}$ and $Da = 10^{-5}$, respectively, satisfy the criteria (Eqs. (27) and (30)) under the condition of $\varepsilon = 0.9$, $\lambda = 0.1$ and $Ra = 10^8$. As

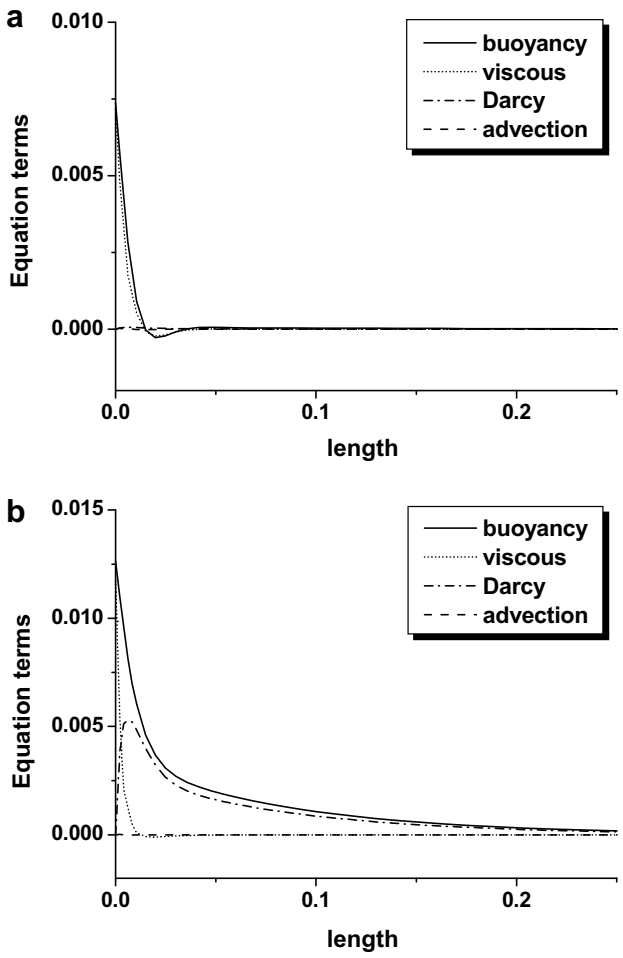

Fig. 3. Comparison of the terms in the vertical momentum equation along the centerline: $\varphi = 30°$, $Bi = 100$, $\lambda = 0.1$. (a) $Ra = 10^8$, $Da = 10^{-3}$ and (b) $Ra = 10^8$, $Da = 10^{-5}$.

is evident, the principal balance of buoyancy–viscous effect is discernible for Eq. (27), while the buoyancy term is balanced with the Darcy term for Eq. (30) in much of the thermal boundary layer except the near-wall region, in which the viscous term is dominant.

3.3. Criteria for local thermal equilibrium

As described in Ref. [16], the assumption of local thermal equilibrium is reasonable when the system satisfies the following criterion:

$$\frac{(\rho c)_f \varepsilon}{h_{sf}a_{sf}t} \ll 1, \tag{31}$$

where t denotes the required time scale for the fluid near the heating wall to travel to the cooling wall. Since the fluid circulates along the walls, the time scale can be expressed as

$$t \sim \frac{H}{v}, \tag{32}$$

where H and v represent the height of cavity and velocity scale in the y-direction, respectively. With the definition

of the Biot number in Eq. (8), i.e., $Bi = h_{sf}a_{sf}H^2/k_e$, and Eq. (32), the criterion (Eq. (31)) can be rearranged as

$$\frac{\varepsilon vH}{\kappa_e Bi} \ll 1. \tag{33}$$

By substituting the velocity scales (Eqs. (25) and (29)) into the criterion (Eq. (33)), the criteria for local thermal equilibrium are rewritten as

$$\varepsilon^{3/2}\left(\frac{Ra}{1+\lambda}\right)^{1/2}\frac{1}{Bi} \ll 1, \tag{34}$$

$$\frac{\varepsilon Ra_m}{Bi} \ll 1. \tag{35}$$

In the above, Eqs. (34) and (35) are the criteria in the buoyancy–viscous and buoyancy–Darcy regimes, respectively.

3.4. Effect of Rayleigh number in the buoyancy–viscous regime

Fig. 4 illustrates the impact of Ra on LTD_{max} in the buoyancy–viscous regime. The setup of $Ra = 10^6$, 10^7 and 10^8, under the condition of $\varphi = 45°$, $Bi = 10$, $\lambda = 0.5$ and $Da = 10^{-2}$, satisfies the criterion (Eq. (27)). As Ra increases, the fluid phase becomes more stratified due to the stronger convective effect. However, the temperature distributions of solid phase, in which the conductive heat transfer dominates, are largely unchanged even though Ra is increased. Therefore, LTD_{max} increases with Ra and φ due to intense flow motions. This implies that the assumption of local thermal equilibrium becomes less valid as Ra increases, which corresponds to the criterion for local thermal equilibrium (Eq. (34)). As shown in Fig. 5, the heat transfer enhancement by the non-vertical sidewalls is apparent in both the one-equation model and the two-equation model. However, the mean Nusselt number $\overline{Nu}$ of the two-equation model is lower than $\overline{Nu}$ of the one-equation model since the solid phase is less stratified than the fluid phase in the two-equation model. The deviation

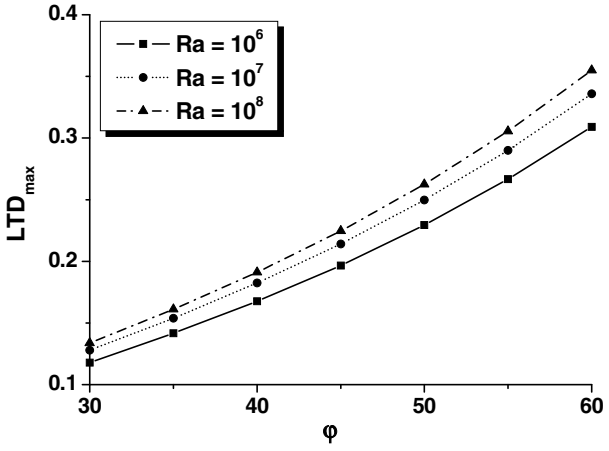

Fig. 4. Maximum value of the local temperature difference versus the incline angle: $Bi = 10$, $\lambda = 0.5$, $Da = 10^{-2}$.

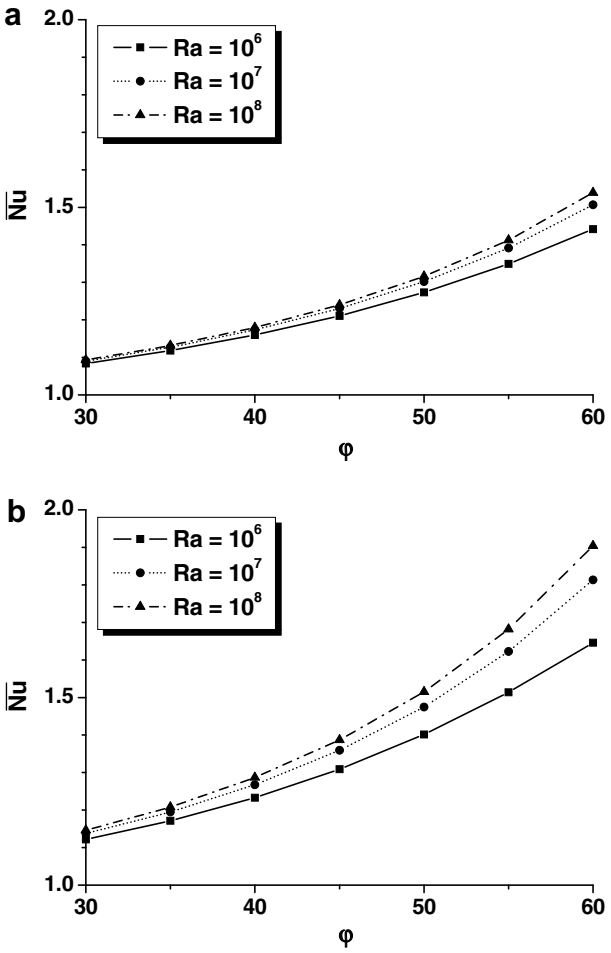

Fig. 5. Mean Nusselt number at the cooling wall versus the incline angle: $Bi = 10$, $\lambda = 0.5$, $Da = 10^{-2}$. (a) Two-equation model and (b) one-equation model.

between the one-equation model and the two-equation model results becomes significant as Ra and φ increase. The heat transfer in the solid phase tends to be overpredicted in the one-equation model as the convective effect intensifies.

3.5. Effective fluid-to-solid thermal conductivity ratio in the buoyancy–viscous regime

Fig. 6 shows the impact of λ on LTD_{max} in the buoyancy–viscous regime. The setup of $\lambda = 0.1$ and $\lambda = 1.0$, under the condition of $\varphi = 45°$, $Bi = 10$, $Ra = 10^7$ and $Da = 10^{-3}$, satisfies the criterion (Eq. (27)). As seen in the definition of λ in Eq. (8), a larger λ indicates that the conductivity of the solid phase, relative to the fluid phase, decreases. Therefore, the solid temperature profile becomes more stratified as λ increases. The convective effect penetrates more easily into the solid phase at high λ. For this reason, LTD_{max} diminishes as λ increases, which indicates that the temperature distributions approach the local thermal equilibrium. This result confirms the above-stated criterion (Eq. (34)). Hence, as demonstrated in Fig. 7, the one-

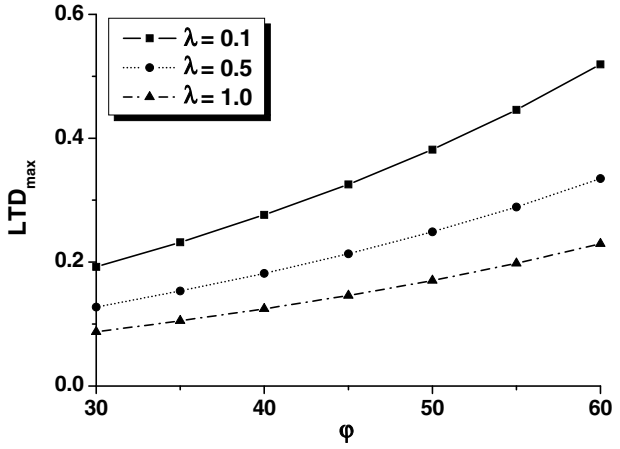

Fig. 6. Maximum value of the local temperature difference versus the incline angle: $Bi = 10$, $Ra = 10^7$, $Da = 10^{-3}$.

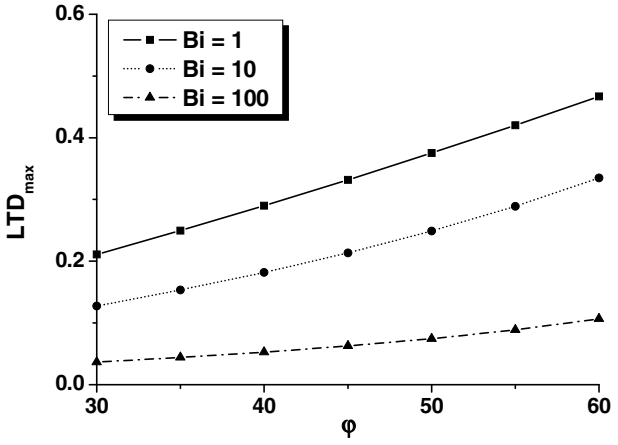

Fig. 8. Maximum value of the local temperature difference versus the incline angle: $\lambda = 0.5$, $Ra = 10^7$, $Da = 10^{-3}$.

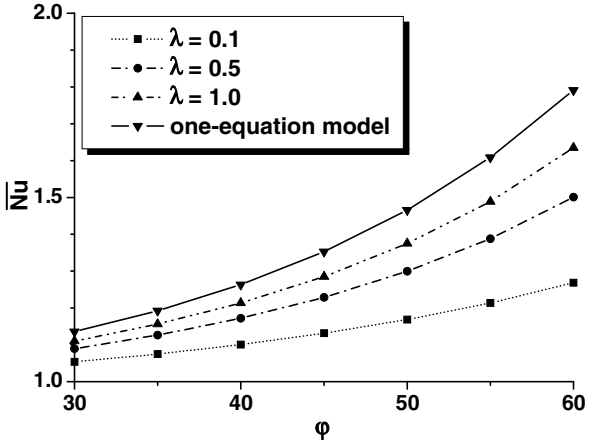

Fig. 7. Mean Nusselt number at the cooling wall versus the incline angle: $Bi = 10$, $Ra = 10^7$, $Da = 10^{-3}$.

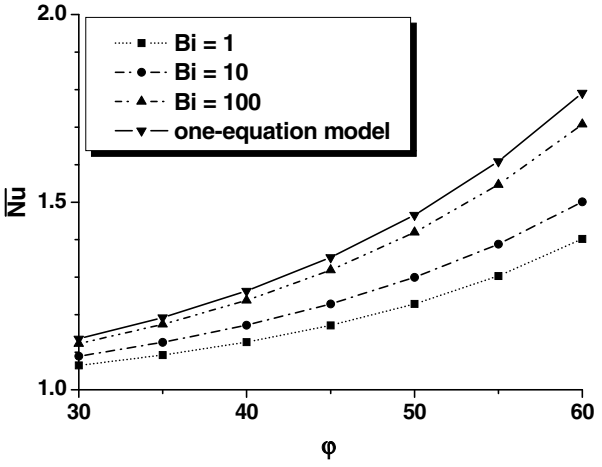

Fig. 9. Mean Nusselt number at the cooling wall versus the incline angle: $\lambda = 0.5$, $Ra = 10^7$, $Da = 10^{-3}$.

equation model is a limiting case of the two-equation model since the difference between the two models decreases as λ increases.

3.6. Effect of the Biot number in the buoyancy–viscous regime and buoyancy–Darcy regime

The impact of Bi on $\mathrm{LTD}_{\max}$ in the buoyancy–viscous regime is highlighted in Fig. 8. The setup of $Bi = 1$, $Bi = 10$ and $Bi = 100$ is considered under the condition of $\varphi = 45°$, $\lambda = 0.5$, $Ra = 10^7$ and $Da = 10^{-3}$. This satisfies the criterion (Eq. (27)). The solid temperature distribution approaches the fluid temperature distributions as Bi increases. This indicates that the solid phase becomes more stratified. This trend is attributed to the enhanced communication between the two phases. Hence, as illustrated in Fig. 8, $\mathrm{LTD}_{\max}$ decreases as Bi increases, which indicates that the local thermal equilibrium is approached. The numerical results are supportive of the criterion (Eq. (34)). In Fig. 9, it is discernible that the one-equation model can be a limiting case of the two-equation model. Also, the one-equation model gives correct solutions at high Bi, because the assumption of the local thermal equilibrium is valid at high Bi. The impact of Bi in the buoyancy–Darcy regime is also consistent with the criterion (Eq. (35)).

3.7. Effect of modified Rayleigh number in the buoyancy–Darcy regime

Fig. 10 shows the impact of Ra_{m} on $\mathrm{LTD}_{\max}$ in the buoyancy–Darcy regime under the condition of $\varphi = 45°$, $Bi = 1$ and $\lambda = 0.5$. As Ra_{m} increases, the stratification of the fluid phase intensifies by the stronger flow motion. However, changes are small in the solid temperature distributions as Ra_{m} varies, since conductive heat transfer is dominant in the solid phase. When Ra_{m} is fixed, the stratification of temperature in both phases is slightly enhanced as Ra increases

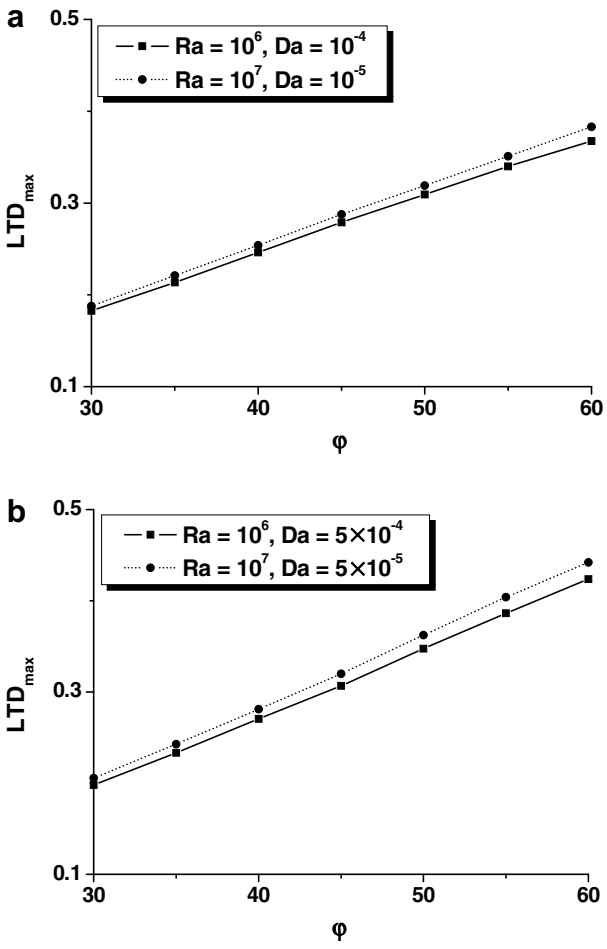

Fig. 10. Maximum value of the local temperature difference versus the incline angle: $Bi = 1$, $\lambda = 0.5$. (a) $Ra_m = 100$ and (b) $Ra_m = 500$.

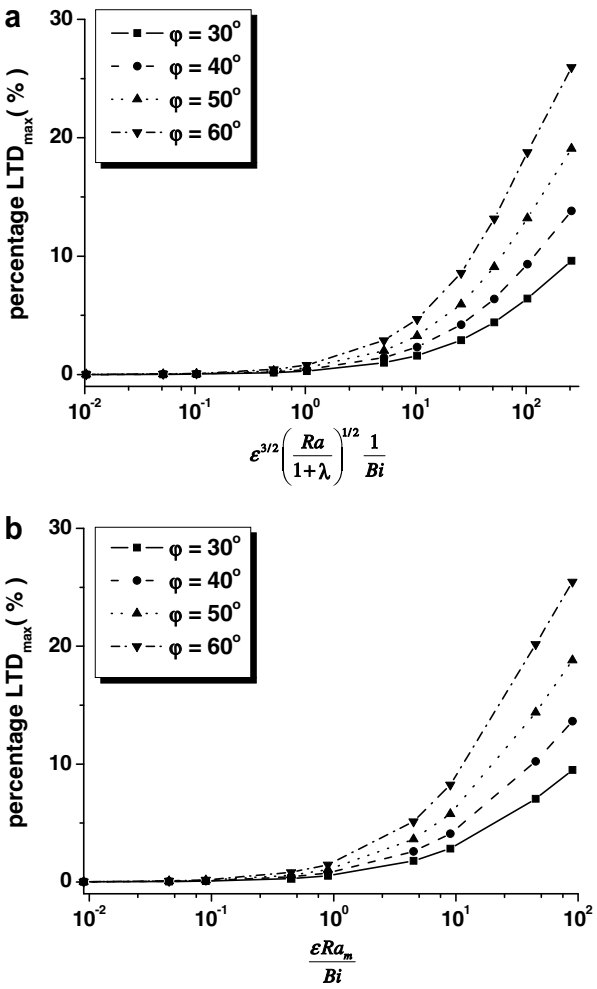

Fig. 11. Percentage LTD_{max} (%) with the value of the criterion: (a) Buoyancy–viscous regime and (b) Buoyancy–Darcy regime.

(Da decreases). As shown in Fig. 10, this trend brings forth an increase of LTD_{max} with Ra_m and φ, due to the stronger convective effect. When Ra_m is fixed, LTD_{max} increases as Ra increases (Da decreases). These results indicate that the assumption of local thermal equilibrium becomes adequate as Ra_m decreases. This is in line with the criterion for the local thermal equilibrium (Eq. (35)).

3.8. Validity of criteria for local thermal equilibrium

In order to validate the proposed criteria for local thermal equilibrium (Eqs. (34) and (35)), Percentage LTD_{max} is presented in Fig. 11. The condition of local thermal equilibrium is approached when the value of the left-hand side of the criterion is less than 1, since Percentage LTD_{max} is less than 2% in the both regimes. However, the assumption of local thermal equilibrium is less valid when it is lager than 1 because Percentage LTD_{max} increases rapidly with it. Furthermore, the lager Percentage LTD_{max} appears when the incline angle of the sidewalls is larger, due to the stronger convective effect. The proposed criteria (Eqs. (34) and (35)) are in line with the numerical results in Fig. 11.

4. Conclusions

Numerical results are acquired to scrutinize the buoyant convection in a parallelogrammic enclosure filled with a porous medium. The inclination of the insulating sidewalls gives rise to convective fluid flow by local baroclinicity in the immediate neighborhood of the non-vertical sidewalls. For a positive incline angle φ, a counter-clockwise circulation cell occupies the cavity. The fluid flows are concentrated to the boundary layers on the wall at high Ra_m while the fluid is mostly motionless and is in a nearly vertical stratification in the interior. Enhancement of the heat transfer is more pronounced as Ra_m and φ increase.

The general criteria for the validity of local thermal equilibrium assumption are discussed by a scale analysis in the governing equations. The effect of parameters used in the criteria is, respectively, investigated for the buoyancy–viscous regime and the buoyancy–Darcy regime. The one-equation model is viewed to be a limiting case of the two-equation model when the condition of local thermal equilibrium is approached. The numerical results show

that the effect of relevant parameters is well predicted by the proposed criteria.

Acknowledgement

This work was supported by the Brain Korea 21 Project in 2007.

References

[1] M. Kaviany, Principles of Heat Transfer in Porous Media, second ed., Springer, New York, 1991.
[2] D.A. Nield, A. Bejan, Convection in Porous Media, third ed., Springer, New York, 2006.
[3] D.B. Ingham, I. Pop (Eds.), Transport Phenomena in Porous Media, vol. II, Pergamon, Oxford, 2002.
[4] J. Patterson, J. Imberger, Unsteady natural convection in a rectangular cavity, J. Fluid Mech. 100 (1980) 65–86.
[5] S.G. Schladow, J.C. Patterson, R.L. Street, Transient flow in a side-heated cavity at high Rayleigh number: a numerical study, J. Fluid Mech. 200 (1989) 121–148.
[6] D. Poulikakos, A. Bejan, Unsteady natural convection in a porous layer, Phys. Fluids 26 (5) (1983) 1183–1191.
[7] S.W. Hsiao, Natural convection in an inclined porous cavity with variable porosity and thermal dispersion effects, Int. J. Numer. Methods Heat Fluid Flow 8 (1) (1998) 97–117.
[8] A.M. Al-Amiri, Analysis of momentum and energy transfer in a lid-driven cavity filled with a porous medium, Int. J. Heat Mass Transfer 43 (2000) 3513–3527.
[9] A.A. Merrikh, A.A. Mohamad, Non-Darcy effects in buoyancy driven flows in an enclosure filled with vertically layered porous media, Int. J. Heat Mass Transfer 45 (2002) 4305–4313.
[10] G.B. Kim, J.M. Hyun, H.S. Kwak, Buoyant convection in a square cavity partially filled with a heat-generating porous medium, Numer. Heat Transfer, Part A 40 (2001) 601–618.
[11] G.B. Kim, J.M. Hyun, Buoyant convection of a power-law fluid in an enclosure filled with heat-generating porous media, Numer. Heat Transfer, Part A 45 (2004) 569–582.
[12] E. Holzbecher, Free convection in open-top enclosures filled with a porous medium heated from below, Numer. Heat Transfer, Part A 46 (2004) 241–254.
[13] K.H. Kim, J.M. Hyun, J.W. Kim, Transient buoyant convection in a porous-medium enclosure by sudden imposition of gravity, J. Porous Media 8 (3) (2005) 311–326.
[14] K. Slimi, A. Mhimid, M.B. Salah, S.B. Nasrallah, A.A. Mohamad, L. Storesletten, Anisotropy effects on heat and fluid flow by unsteady natural convection and radiation in saturated porous media, Numer. Heat Transfer, Part A 48 (2005) 763–790.
[15] T. Basak, S. Roy, H.S. Takhar, Effects of nonuniformly heated wall(s) on a natural-convection flow in a square cavity filled with a porous medium, Numer. Heat Transfer, Part A 51 (2007) 959–978.
[16] S.J. Kim, S.P. Jang, Effects of the Darcy Number, the Prandtl number, and the Reynolds number on local thermal non-equilibrium, Int. J. Heat Mass Transfer 45 (2002) 3885–3896.
[17] S.A. Khashan, A.M. Al-Amiri, I. Pop, Numerical simulation of natural convection heat transfer in a porous cavity heated from below using a non-Darcian and thermal non-equilibrium model, Int. J. Heat Mass Transfer 49 (2006) 1039–1049.
[18] T.S. Lee, Computational and experimental studies of convective fluid motion and heat transfer in inclined non-rectangular enclosures, Int. J. Heat Fluid Flow 5 (1) (1984) 29–36.
[19] T.S. Lee, Numerical experiments with fluid convection in tilted nonrectangular enclosures, Numer. Heat Transfer, Part A 19 (1991) 487–499.
[20] J.M. Hyun, B.S. Choi, Transient natural convection in parallelogram-shapes enclosure, Int. J. Heat Fluid Flow 11 (2) (1990) 129–134.
[21] G.B. Kim, J.M. Hyun, Buoyant convection in a non-rectangular cavity with non-vertical insulating sidewalls, Int. J. Heat Mass Transfer 42 (1999) 2111–2117.
[22] M. Ouriemi, P. Vasseur, A. Bahloul, Natural convection of a binary fluid in a slightly inclined shallow cavity, Numer. Heat Transfer, Part A 48 (2005) 547–565.
[23] V.A.F. Costa, Double-diffusive natural convection in parallelogrammic enclosures, Int. J. Heat Mass Transfer 47 (2004) 2913–2926.
[24] V.A.F. Costa, Double-diffusive natural convection in parallelogrammic enclosures filled with fluid-saturated porous media, Int. J. Heat Mass Transfer 47 (2004) 2699–2714.
[25] A.C. Baytas, I. Pop, Free convection in oblique enclosures filled with a porous medium, Int. J. Heat Mass Transfer 42 (1999) 1047–1057.
[26] A. Misirlioglu, A.C. Baytas, I. Pop, Free convection in a wavy cavity filled with a porous medium, Int. J. Heat Mass Transfer 48 (2005) 1840–1850.
[27] A. Misirlioglu, A.C. Baytas, I. Pop, Natural convection inside an inclined wavy enclosure filled with a porous medium, Transport Porous Media 64 (2006) 229–246.
[28] S.V. Patankar, Numerical Heat Transfer and Fluid Flow, Hemisphere/McGraw-Hill, New York, 1980.
[29] T. Hayase, J.A.C. Humphrey, R. Greif, A consistently formulated QUICK scheme for fast and stable convergence using finite-volume iterative calculation procedures, J. Comput. Phys. 98 (1992) 108–118.